Transition Met Chem (2011) 36:819–827
DOI 10.1007/s11243-011-9536-5

Synthesis, structure, DNA-binding properties, and antioxidant activity of copper(II) and cobalt(II) complexes with bis(*N*-allylbenzimidazol-2-ylmethyl)benzylamine

Hui-Lu Wu · Jing-Kun Yuan · Ying Bai · Fei Jia · Bin Liu · Fan Kou · Jin Kong

Received: 8 June 2011 / Accepted: 6 September 2011 / Published online: 20 September 2011

Abstract Bis(*N*-allylbenzimidazol-2-ylmethyl)benzylamine (babb) and two of its complexes, $[Cu(babb)(pic)_2]\cdot H_2O$ (**1**) and $[Co(babb)_2](pic)_2$ (**2**) (pic = picrate), have been synthesized and characterized by physico-chemical and spectroscopic methods. Single crystal X-ray diffraction revealed that the two complexes have similar distorted octahedral structures, but the degree of distortion and the coordinated atoms are different. The DNA-binding properties of the free ligand and its two complexes have been investigated by electronic absorption, fluorescence, and viscosity measurements. The results suggest that all three compounds bind to DNA via an intercalative binding mode, and their binding affinity for DNA follows the order **2** > **1** > ligand. Additionally, both complexes exhibited potential antioxidant properties in in vitro studies, and complex **1** was the more effective.

Introduction

Transition metal complexes are currently being used to bind and react at specific sequences of DNA in a search for novel chemotherapeutics and DNA probes and for the development of highly sensitive diagnostic agents [1–3]. Therefore, an understanding of how these small molecules bind to DNA will potentially be useful in the design of such new compounds, which can recognize specific sites or conformations of DNA [2–4].

H.-L. Wu (✉) · J.-K. Yuan · Y. Bai · F. Jia · B. Liu · F. Kou · J. Kong
School of Chemical and Biological Engineering, Lanzhou Jiaotong University, Lanzhou 730070, People's Republic of China
e-mail: wuhuilu@163.com

Benzimidazole is a typical heterocyclic ligand with nitrogen as the donor atom. Interest in exploring benzimidazole derivatives and their metal complexes has been increasing, since the recognition that many of these materials may serve as models that minic both the structure and reactivity of metal sites in complex biological systems and can also possess a broad spectrum of biological activity [5, 6]. Due to their privileged structure and properties [7], benzimidazoles and their derivatives exhibit a wide variety of pharmacological activities such as fungicides or antihelminthics, among others [8]. Hence, transition metal complexes containing benzimidazole ligands are a subject of intensive research not only owing to their rich coordination chemistry but also due to a number of established and potential application areas [9, 10].

In previous studies [11–14], we have investigated that the coordinating ability of various benzimidazole ligands. In this study, the synthesis, characterization, and DNA-binding activities of two transition metal complexes with bis(*N*-allylbenzimidazol-2-ylmethyl)benzylamine are presented. According to relevant reports in the literature [15–18], similar transition metal complexes can exhibit antioxidant activity. We therefore also conducted an investigation into the hydroxyl radical scavenging properties of these complexes.

Experimental

C, H, and N elemental analyses were determined using a Carlo Erba 1106 elemental analyzer. Electrolytic conductivity measurements were made with a DDS-307 type conductivity bridge using 3×10^{-3} mol L^{-1} solutions in DMF at room temperature. IR spectra were recorded in the 4,000–400 cm^{-1} region with a Nicolet FT-VERTEX 70 spectrometer using KBr pellets. Electronic spectra were

taken on Lab-Tech UV Bluestar and Spectrumlab 722sp spectrophotometers. Fluorescence spectra were recorded on a LS-45 spectrofluorophotometer. ^{1}H NMR spectra were recorded on a Varian VR300-MHz spectrometer with TMS as an internal standard.

Calf thymus DNA (CT-DNA) and ethidium bromide (EB) were purchased from Sigma. All chemicals used were of analytical grade. All the experiments involving interaction of the ligand and the complexes with CT-DNA were carried out in doubly distilled water buffer containing 5 mM Tris and 50 mM NaCl and adjusted to pH 7.2 with hydrochloric acid. A solution of CT-DNA gave a ratio of UV absorbance at 260 and 280 nm of about 1.8–1.9, indicating that the CT-DNA was sufficiently free of protein [19]. The CT-DNA concentration per nucleotide was determined spectrophotometrically by employing an extinction coefficient of 6,600 M^{-1} cm^{-1} at 260 nm [20].

DNA-binding study

Absorption titration experiments were performed with fixed concentrations of the complexes, while gradually increasing the concentration of CT-DNA. To obtain the absorption spectra, the required amount of CT-DNA was added to both the compound and reference solutions, in order to eliminate the absorbance of CT-DNA itself. From the absorption titration data, the binding constant (K_b) was determined using the equation [21]:

$$[\mathrm{DNA}]/(\varepsilon_a - \varepsilon_f) = [\mathrm{DNA}]/(\varepsilon_b - \varepsilon_f) + 1/K_b(\varepsilon_b - \varepsilon_f)$$

where [DNA] is the concentration of CT-DNA in base pairs, ε_a corresponds to the observed extinction coefficient (Aobsd/[M]), ε_f corresponds to the extinction coefficient of the free compound, ε_b is the extinction coefficient of the compound when fully bound to CT-DNA, and K_b is the intrinsic binding constant. The ratio of slope to intercept in the plot of [DNA]/($\varepsilon_a - \varepsilon_f$) versus [DNA] gave the value of K_b.

The enhanced fluorescence of EB in the presence of DNA can be quenched by the addition of a second molecule [22, 23]. The extent of fluorescence quenching of EB bound to CT-DNA can be used to determine the extent of binding between the second molecule and CT-DNA. Competitive binding experiments were carried out in the buffer by keeping [DNA]/[EB] = 1 and varying the concentrations of the compounds. The fluorescence spectra of EB were measured using an excitation wavelength of 520 nm, and the emission range was set between 550 and 750 nm. The spectra were analyzed according to the classical Stern–Volmer equation [24]:

$$I_0/I = 1 + K_{\mathrm{SV}}[\mathrm{Q}]$$

where I_0 and I are the fluorescence intensities at 599 nm in the absence and presence of the quencher, respectively, K_{sv} is the linear Stern–Volmer quenching constant, and [Q] is the concentration of the quencher. In these experiments [CT-DNA] = 2.5×10^{-3} mol/L, [EB] = 2.2×10^{-3} mol/L.

Viscosity experiments were conducted on an Ubbelodhe viscometer, immersed in a water bath maintained at 25.0 ± 0.1 °C. Titrations were performed for the complexes (3–30 μM), and each compound was introduced into CT-DNA solution (42.5 μM) present in the viscometer. Data were analyzed as $(\eta/\eta_0)^{1/3}$ versus the ratio of the concentration of the compound to CT-DNA, where η is the viscosity of CT-DNA in the presence of the compound and η_0 is the viscosity of CT-DNA alone. Viscosity values were calculated from the observed flow time of CT-DNA-containing solutions corrected from the flow time of buffer alone (t_0), $\eta = (t - t_0)$ [25].

Hydroxyl radical scavenger measurements

Hydroxyl radicals were generated in aqueous media through the Fenton-type reaction [26, 27]. The aliquots of reaction mixture (3 mL) contained 1.0 mL of 0.10 mmol aqueous safranin, 1 mL of 1.0 mmol aqueous EDTA–Fe(II), 1 mL of 3% aqueous H_2O_2, and a series of quantitative microadditions of solutions of the test compound. A sample without the tested compound was used as the control. The reaction mixtures were incubated at 37 °C for 30 min in a water bath. The absorbance was then measured at 520 nm. All the tests were run in triplicate and are expressed as the mean and standard deviation (SD) [28]. The scavenging effect for $OH^{\cdot}$ was calculated from the following expression:

$$\text{Scavenging ratio}\,(\%) = [(A_i - A_0)/(A_c - A_0)] \times 100\%$$

where A_i = absorbance in the presence of the test compound; A_0 = absorbance of the blank in the absence of the test compound; A_c = absorbance in the absence of the test compound, EDTA–Fe(II) and H_2O_2.

Synthesis of babb

Bis(*N*-allylbenzimidazol-2-ylmethyl)benzylamine (babb) was synthesized following a slight modification of the procedure in ref [29]. Bis(2-benzimidazol-2-ylmethyl)benzylamine (7.34 g, 20 mmol) was reacted with potassium (1.56 g, 40 mmol) in tetrahydrofuran (150 mL). Allyl bromide (4.84 g, 40 mmol) was then added. The resulting solution was concentrated and recrystallized from ethanol to give pale yellow block crystals [30]. Yield: 5.46 g (61%); m.p.:113–115 °C. Found (%): C, 77.8; H, 6.5; N, 15.6. Calcd. (%) for $C_{29}H_{29}N_5$: C, 78.0; H, 6.3; N, 15.7. ^{1}H–NMR (DMSO–d_6 400 MHz) δ/ppm: 3.45 (m, 4H, –*CH*$_2$–Ar), 3.85 (s, 4H, –*CH*$_2$–benzimidazol), 4.87–5.68 (m, 10H, –*CH*$_2$–*CH*=*CH*$_2$), 7.22 (m, 5H, H–benzene ring), 7.27–7.64 (m, 8H, H–benzimidazol ring). UV–vis (λ, nm): 279, 286. FTIR (KBr ν/cm^{-1}): 737, ν(*o*–Ar), 1,265, ν(C–N); 1,461, ν(C=N), 1,643, ν(C=C).

Preparation of complex **1**

To a stirred solution of babb (223.5 mg, 0.25 mmol) in hot EtOH (10 mL) was added $Cu(pic)_2$ (129.94 mg, 0.50 mmol) in EtOH (2 mL). A yellow crystalline product formed rapidly. The precipitate was filtered off, washed with EtOH and absolute Et_2O, and dried under vacuum. The crude product was dissolved in MeCN to form a yellow solution into which Et_2O was allowed to diffuse at room temperature. Yellow crystals of **1** suitable for X-ray measurement were obtained after several weeks. Yield: 160.5 mg (64%). Found (%): C, 49.9; H, 3.5; N, 15.6. Calcd. (%) for $C_{41}H_{35}CuN_{11}O_{15}$: C, 49.7; H, 3.7; N, 15.5. Λ_m(DMF, 297 K): 77.9 S cm^2 mol^{-1}. UV–vis (λ, nm): 275, 280, 381. FTIR (KBr ν/cm^{-1}): 746, ν(*o*–Ar); 1,269, ν(C–N); 1,363, ν(O–N–O); 1,481, ν(C=N), 1,635, ν(C=C) [30].

Preparation of complex **2**

Complex **2** was prepared by a similar procedure as for complex **1**, using $Co(pic)_2$ instead of $Cu(pic)_2$. Yield: 250.3 mg (63%). Found (%): C, 70.1; H, 6.2; N, 14.3 Calcd. (%) for $C_{70}H_{62}CoN_{16}O_{14}$: C, 70.3; H, 6.3; N, 14.1. Λ_m(DMF, 297 K): 133.04 S cm^2 mol^{-1}. UV–vis (λ, nm): 281, 381. FTIR (KBr ν/cm^{-1}): 746, ν(*o*–Ar); 1,269, ν(C–N); 1,366, ν(O–N–O); 1,483 cm^{-1}, ν(C=N), 1,633 cm^{-1}, ν(C=C) [30].

X-ray crystallography

A suitable single crystal was mounted on a glass fiber, and the intensity data were collected on a Bruker Smart CCD diffractometer with graphite-monochromated Mo–K_α radiation ($\lambda = 0.71073$ Å) at 296 K. Data reduction and cell refinement were performed using the SMART and SAINT programs [31]. The structure was solved by direct methods and refined by full-matrix least-squares against F^2 of data using SHELXTL software [32]. All H atoms were found in difference electron maps and subsequently refined in a riding-model approximation with C–H distances ranging from 0.93 to 0.97 Å and $U_{iso}(H) = 1.2\ U_{eq}(C)$. Basic crystal data, description of the diffraction experiment, and details of the structure refinement are given in Table 1. Selected bond distances and angles are presented in Table 2.

Results and discussion

Characterization and structures of the complexes

The two complexes are soluble in DMF, DMSO, and acetonitrile, but insoluble in water and other organic solvents, such as methanol, ethanol, petroleum ether, trichloromethane, etc. The elemental analyses show that their compositions are $[Cu(babb)(pic)_2]\cdot H_2O$, and $[Co(babb)_2](pic)_2$. The electrolytic conductivity of complex **2** shows that it is 1:2 electrolyte in DMF [33]. In theory, complex **1** is neutral, but the conductivity shows that it is a 1:1 electrolyte in DMF, which may be attributed to partial ionization of the discrete $[Cu(babb)(pic)_2]$ in the DMF.

The IR spectra of the two complexes are closely related to that of the free ligand babb. One of the most diagnostic changes occurs in the region between 1,650 and 1,250 cm^{-1}. The spectrum of free babb shows a strong band at 1,462 cm^{-1} and weak bands at 1,643 and 1,408 cm^{-1}, attributable to the ν(C=N) and ν(C=C) frequencies of the benzimidazole group [34–37], respectively. The location of these two bands was slightly shifted for both complexes; the band at 1,462 cm^{-1} is shifted to 1,481 and 1,483 cm^{-1} for complexes, respectively, which implies direct coordination of all four imine nitrogen atoms to the central metal atom [38]. Information regarding the possible bonding modes of the picrate and benzimidazole rings may also be obtained from the IR spectra [39].

DMF solutions of the ligand and its complexes show, as expected, almost identical UV spectra. The UV bands of the free ligand (286, 279 nm) are only marginally red-shifted (5–6 nm) for complex **1**, which is evidence of C=N coordination to the metal center. These bands are assigned to $\pi \rightarrow \pi^*$ (imidazole) transitions [12]. Conversely, the bands are marginally blue-shifted (5–6 nm) for complex **2,** this phenomenon also shows that C=N is involved in coordination to the metal center [40]. The picrate bands (observed at 381 nm both complexes) are assigned to $n \rightarrow \pi^*$ and $\pi \rightarrow \pi^*$ transitions [11].

X-ray structures of the complexes

The crystal structure of complex **1** consists of discrete $[Cu(babb)(pic)_2]$ and solvent water molecules. The solvent water molecules are present in the crystal lattice, but have no direct interactions with the $[Cu(babb)(pic)_2]$. The ORTEP structure (30% probability ellipsoids) of $[Cu(babb)(pic)_2]$ with atom numberings is shown in Fig. 1.

The central copper(II) atom is six-coordinate with a CuN_3O_3 environment. The ligand acts as a tridentate N-donor, with the remaining coordination sites occupied by three O atoms from two picrates. The coordination geometry of the Cu(II) may be best described as distorted octahedral with (O1, O2, O8, N1) providing the equatorial plane. The maximum deviation distance (N1) from the least-squares plane calculated from the four coordination atom atoms is 0.19 Å, indicating that those atoms are almost in a plane. The average bond length between the copper and the apical nitrogen atoms (N3, N5) is 1.975(3) Å, which is about 0.247 Å shorter than the bond average length between the copper and the four coordinated

Table 1 Crystal and structure refinement data for complex [Cu(babb) $(pic)_2]\cdot H_2O$ (**1**) and $[Co(babb)_2](pic)_2$ (**2**)

Complex	**1**	**2**
Molecular formula	$C_{41}H_{35}CuN_{11}O_{15}$	$C_{70}H_{62}CoN_{16}O_{14}$
Molecular weight	985.34	1,410.29
Crystal system	Monoclinic	Triclinic
Space group	P21/c	P-1
a (Å)	13.960(8)	13.9512(16)
b (Å)	14.369(8)	13.9610(17)
c (Å)	24.633(11)	19.159(2)
α (°)	90	89.6910(10)
β (°)	112.59(2)	69.8690(10)
γ (°)	90	74.0040(10)
V (Å^3)	4,562(4)	3,351.4(7)
Z	4	2
ρ_{cald} (mg m^{-3})	1.435	1.398
F (000)	2,028	1,466
Crystal size (mm)	0.33 × 0.31 × 0.28	0.40 × 0.38 × 0.30
θ range for data collection (°)	2.12–25.50	2.28–25.00
$h/k/l$ (max, min)	−11,16/−17,17/−29,28	−16,15/−16,16/−22,19
Reflections collected	22,789	23,116
Independent reflections	8,412 [R (int) = 0.0451]	11,656 [R (int) = 0.0264]
Refinement method	Full-matrix least-squares on F^2	Full-matrix least-squares on F^2
Data/restraints/parameters	8,412/11/613	11,656/41/910
Goodness-of-fit on F^2	1.045	1.019
Final R_1, wR_2 indices [I > 2σ (I)]	0.0656, 0.1922	0.0561, 0.1485
R_1, wR_2 indices (all date)	0.1137, 0.2325	0.0888, 0.1759
Largest differences peak and hole (e Å^{-3})	1.637 and −0.517	0.809 and −0.562

nitrogen atoms in the equatorial plane. The bond angle of the two atoms (N3–Cu–N5) in axial positions is 163.52(14)°. Therefore, the geometry around the Cu(II) is a distorted octahedron [41–44].

The crystal structure of complex **2** consists of discrete $[Co(babb)_2]^{2+}$ cations and two picrate anions which surround the $[Co(babb)_2]^{2+}$. The ORTEP structure (30% probability ellipsoids) of the $[Co(babb)_2]^{2+}$ with atom numberings is shown in Fig. 2.

The crystal structure of complex **2** is similar to that of complex **1**. The equatorial plane is provided by atoms N1, N3, N6, and N7, where the largest deviation from the mean plane is 0.356 Å, and the Co atom is out of this plane by only 0.014 Å. The axial positions are occupied by the atoms N5 and N9. The distances between the axial atoms N5, N9, and the equatorial plane are 2.033 Å and 2.038 Å, respectively. The bond angle formed the two axial atoms (N5–Co–N9) is 145.31(11)°. The most obvious difference between complexes **1** and **2** is the different degree of deformation from a regular octahedron, which is apparently caused by the steric effect of the ligand. The coordination geometry of complex **1** is much closer to regular octahedral.

DNA-binding properties

Electronic absorption spectroscopy has been widely employed to determine the binding characteristics of metal complexes with DNA [45–47]. We have investigated the binding mode of DNA with these complexes through absorption titration experiments. The absorption spectra of the free ligand and complexes **1** and **2** in the absence and presence of CT-DNA (at a constant concentration of complex) are given in Fig. 3. With increasing DNA concentrations, the hypochromisms are 18.3% at 275 nm for free babb; 20.2% at 280 nm for complex **1**; and 35.4% at 281 nm for complex **2**. The λ_{max} for free babb increased from 275 to 276, while that for the complex **1** increased from 280 to 282 nm and that for complex **2** increased from 281 to 282 nm, i.e., slight red shifts of about 1–2 nm under identical experimental conditions. The hypochromism suggested that the compounds interact with CT-DNA [48]. The K_b values of free babb and complexes **1** and **2** were 2.26×10^3 M^{-1} (R = 0.98 for 15 points), 7.92×10^4 M^{-1} (R = 0.98 for 6 points in the linear part), and 9.49×10^4 M^{-1} (R = 0.99 for 16 points), respectively. Hence, the binding strength of complex **2** is greater than that of complex **1** and the free ligand.

Table 2 Selected bond distances (Å) and angles (°) in complex **1** and **2**

Complex	**1**		**2**	
Bond distances	Cu–O(1)	1.958(3)	Co(1)–N(3)	2.075(3)
	Cu–N(5)	1.968(3)	Co(1)–N(7)	2.109(3)
	Cu–N(3)	1.981(3)	Co(1)–N(9)	2.129(3)
	Cu–N(1)	2.101(3)	Co(1)–N(5)	2.147(3)
	Cu–O(8)	2.385(3)	Co(1)–N(6)	2.410(3)
	Cu–O(2)	2.444(4)	Co(1)–N(1)	2.529(3)
Bond angles	O(1)–Cu–N(5)	97.31(14)	N(3)–Co(1)–N(7)	103.75(11)
	O(1)–Cu–N(3)	99.16(13)	N(3)–Co(1)–N(9)	96.04(10)
	N(5)–Cu–N(3)	163.52(14)	N(7)–Co(1)–N(9)	106.58(11)
	O(1)–Cu–N(1)	176.33(12)	N(3)–Co(1)–N(5)	102.04(11)
	N(5)–Cu–N(1)	81.51(14)	N(7)–Co(1)–N(5)	97.60(11)
	N(3)–Cu–N(1)	82.08(13)	N(9)–Co(1)–N(5)	145.31(11)
	O(1)–Cu–O(8)	98.77(11)	N(3)–Co(1)–N(6)	168.55(10)
	N(5)–Cu–O(8)	90.05(12)	N(7)–Co(1)–N(6)	76.04(10)
	N(3)–Cu–O(8)	86.98(12)	N(9)–Co(1)–N(6)	73.31(9)
	N(1)–Cu–O(8)	84.73(11)	N(5)–Co(1)–N(6)	89.29(10)
	O(1)–Cu–O(2)	77.24(12)	N(3)–Co(1)–N(1)	74.29(10)
	N(5)–Cu–O(2)	89.15(16)	N(7)–Co(1)–N(1)	167.16(10)
	N(3)–Cu–O(2)	94.93(16)	N(9)–Co(1)–N(1)	86.26(10)
	N(1)–Cu–O(2)	99.24(12)	N(5)–Co(1)–N(1)	70.81(10)
	O(8)–Cu–O(2)	175.79(11)	N(6)–Co(1)–N(1)	108.46(9)

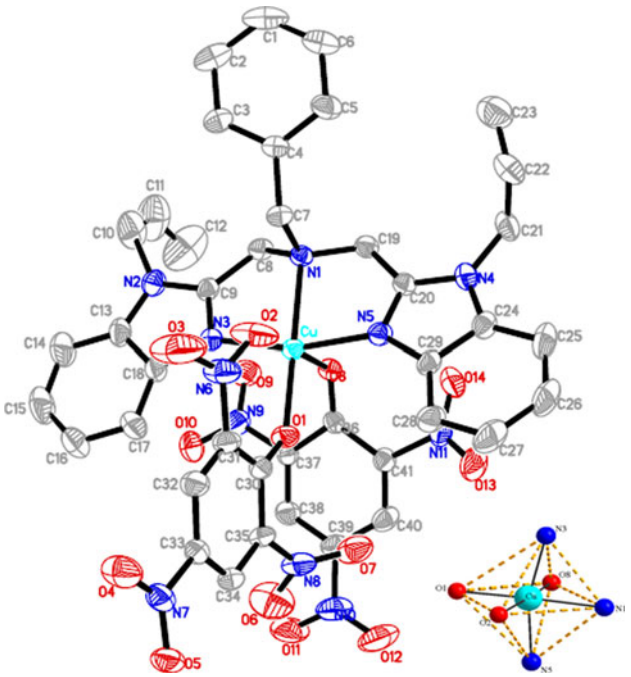

Fig. 1 Molecular structure and atom numberings of $[Cu(babb)(pic)_2]$ with hydrogen atoms and solvent water molecule omitted for clarity

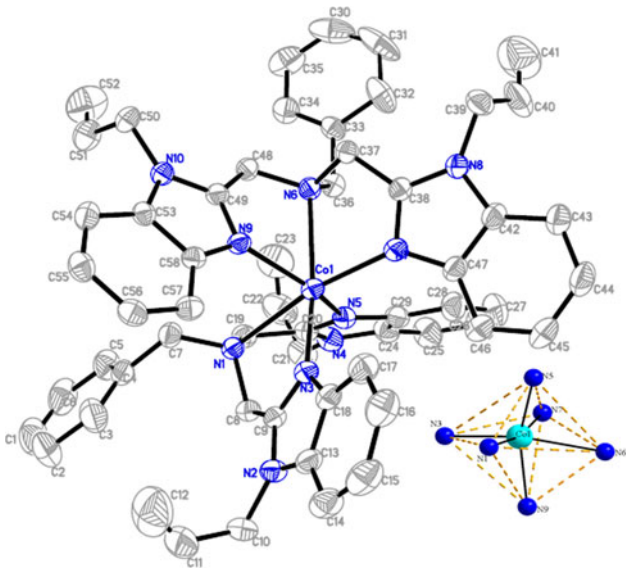

Fig. 2 Molecular structure and atom numberings of the $[Co(babb)_2]^{2+}$ with hydrogen atoms omitted for clarity

Considering these experimental results, we speculate that the planar elements of the structures, for example, benzene rings, have a direct effect on the affinity for DNA, $\pi \rightarrow \pi^*$ stacking interactions; increasing numbers of benzene rings may lead to higher affinity for DNA, which is consistent with the experimental results. In addition, electrostatic attraction may be another reason for the different affinities for DNA. Since $[Cu(babb)(pic)_2]$ is neutral, while $[Co(babb)_2]^{2+}$ is a cation, electrostatic interactions will

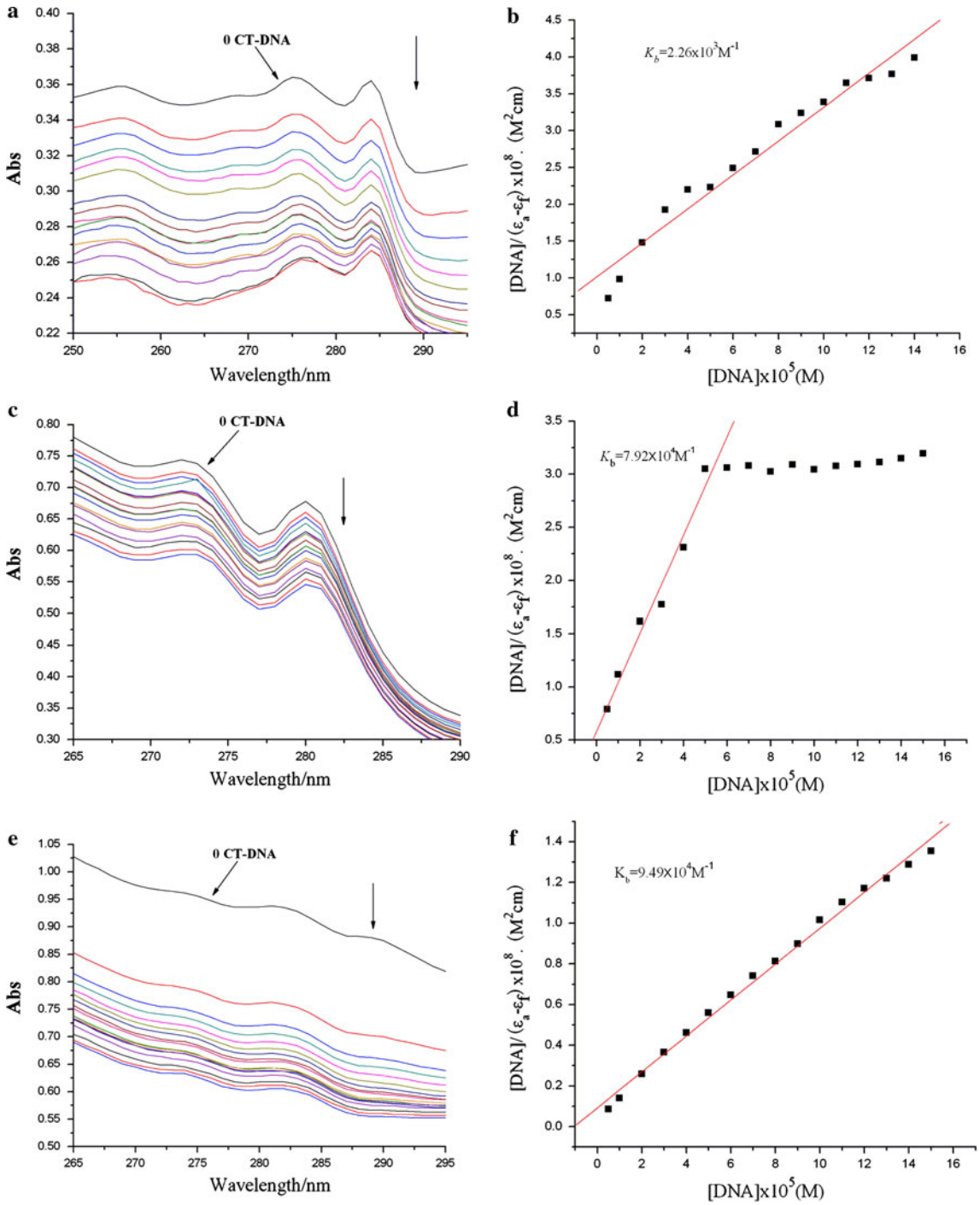

Fig. 3 Electronic spectra of **a** free babb, **c** complex **1**, and **e** complex **2** in Tris–HCl buffer upon addition of CT-DNA. [Compound] = 3×10^{-5} M^{-1}, [DNA] = 2.5×10^{-5} M^{-1}. The *arrow* shows the emission intensity changes upon increasing DNA concentration. *Plots* of [DNA]/(ε_a–ε_f) versus [DNA] for the titration of **b** ligand, **d** complex **1** and **f** complex **2** with CT-DNA

help to strengthen the interactions between the complex and DNA.

In general, measurement of the ability of a complex to affect the intensity of EB fluorescence in the EB-DNA adduct allows determination of the affinity of the complex for DNA, whatever the binding mode may be. If a complex can displace EB from DNA, the fluorescence of the solution will be reduced due to the fact that free EB molecules are readily quenched by the solvent water [49]. For all the compounds, no emission was observed either alone or in

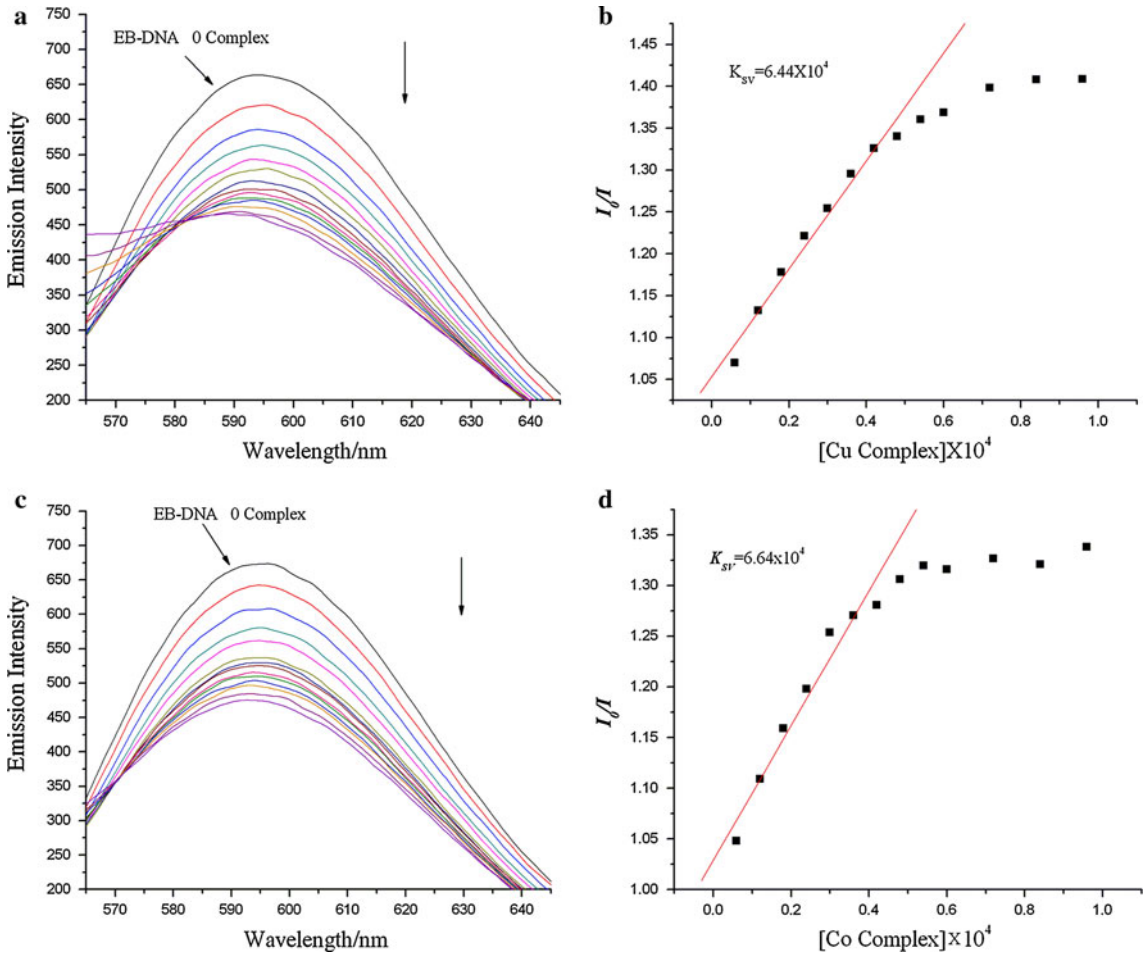

Fig. 4 Emission spectra of EB bound to CT-DNA in the presence of complexes **1** (**a**) and **2** (**c**); [Complex] = 3 × 10^{-5} M; λ_{ex} = 520 nm. The *arrows* show the intensity changes upon increasing concentrations of the complexes. Fluorescence quenching curves of EB bound to CT-DNA by complexes **1** (**b**) and **2** (**d**). (*Plots* of I_0/I versus [Complex])

the presence of CT-DNA in the buffer. The addition of the free ligand does not produce any significant changes of the intensity or position of the band at 599 nm of the DNA-EB system, indicating that free babb cannot displace EB from the DNA-EB complex. The fluorescence quenching of DNA–bound EB by the complexes **1** and **2** is shown in Fig. 4. The behavior of both complexes is in good agreement with the Stern–Volmer equation, which provides further evidence that the complexes bind to DNA. The K_{sv} values for complexes **1** and **2** are 6.44 × 10^4 (R = 0.98 for 8 points) and 6.64 × 10^4 M^{-1} (R = 0.98 for 7 points), respectively. The data suggest that the interaction of complex **2** with CT-DNA is stronger than that of complex **1**, consistent with the UV-V is results discussed above.

Hydrodynamic measurements that are sensitive to DNA length changes are regarded as the least ambiguous and most critical tests of a binding model in solution in the absence of crystallographic structural data [50, 51]. For the

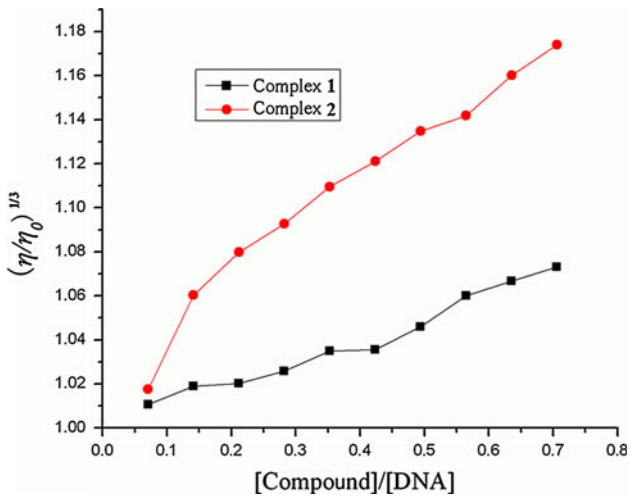

Fig. 5 Effect of increasing amounts of the compounds on the relative viscosity of CT-DNA at 25.0 ± 0.1 °C

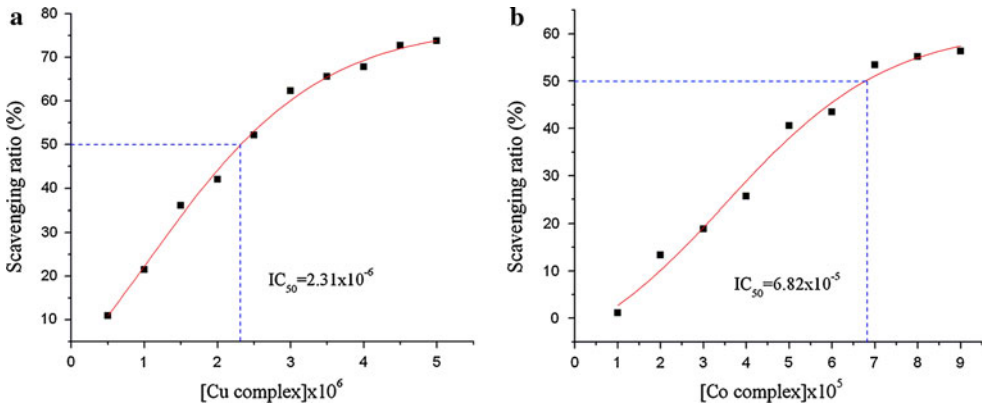

Fig. 6 The inhibitory effect of complexes **1** (**a**) and **2** (**b**) on $OH^{\cdot}$ radicals; the suppression ratio increases with increasing concentration of the test compound

free ligand and the complexes, as increasing amounts of the compounds are added, the viscosity of DNA increases steadily. The values of $(\eta/\eta_0)^{1/3}$ were plotted against [compound]/[DNA]. In classical intercalation, the DNA helix lengthens as base pairs are separated to accommodate the bound ligand, leading to increased DNA viscosity, whereas a partial, nonclassical ligand intercalation causes a bend (or kink) in the DNA helix and so reduces its effective length and thereby its viscosity [19].

The effects of the two complexes on the viscosity of CT-DNA are shown in Fig. 5. The viscosity of CT-DNA increased steadily with the increasing amounts of the complex, providing further evidence that the two complexes intercalate with CT-DNA [52]. The results from the viscosity experiments also demonstrate that the binding strength of complex **2** is greater than that of complex **1**.

Antioxidant activity

We compared the abilities of the present compounds to scavenge hydroxyl radicals with those of the well-known natural antioxidants mannitol and vitamin C, using the same method as reported in a previous study [53]. The 50% inhibitory concentration (IC_{50}) value of mannitol and vitamin C are about 9.6×10^{-3} and 8.7×10^{-3} M^{-1}, respectively. According to the antioxidant experiments, the IC_{50} values of complexes **1** and **2** are 2.31×10^{-6} M^{-1}, 6.82×10^{-5} M^{-1}, respectively, (Fig. 6), which implies that complex **1** exhibits better scavenging activity than complex **2**, as well as mannitol and vitamin C. We suggest that the mechanism of action of complex **1** involves the redox process of copper (Cu^{2+}/Cu^{+}) [54, 55].

Conclusion

In this work, the new ligand bis(*N*-allylbenzimidazol-2-ylmethyl)benzylamine and its Cu(II) and Co(II) complexes have been synthesized and characterized. The binding modes of these compounds with CT-DNA have been studied. The photophysical and viscosity measurements indicate that the compounds interact with CT-DNA through intercalative binding. In addition, their affinity to DNA follows the order **2** > **1** > babb, which can be attributed to a more planar structure upon coordination to the metal. The antioxidant activities of the compounds were also investigated, and the results show that complex **1** exhibits effective scavenging of hydroxyl radicals.

Supplementary data

Crystallographic data (excluding structure factors) for the structures reported in this study have been deposited with the Cambridge Crystallographic Data Center with reference numbers CCDC 827273 and 827272. Copies of the data can be obtained, free of charge, on application to the CCDC, 12 Union Road, Cambridge CB2 1EZ, UK. Tel: +44-01223-762910; fax: +44-01223-336033; e-mail: deposit@ccdc.cam.ac.uk or http://www.ccdc.cam.ac.uk.

Acknowledgments The authors acknowledge the financial support and grant from 'Qing Lan' Talent Engineering Funds by Lanzhou Jiaotong University. The grant from 'Long Yuan Qing Nian' of Gansu Province also is acknowledged.

References

1. Diaz-Cruz MS, Mendieta J, Monjonelli A, Tauler R, Esteban M (1998) J Inorg Biochem 70:91–97
2. Erkkila KE, Odom DT, Barton JK (1999) Chem Rev 99: 2777–2795
3. Ji LN, Zou XH, Lin JG (2001) Coord Chem Rev 216–217:513–536
4. Zeglis BM, Pierre VC, Barton JK (2007) Chem Commun 44: 4565–4579
5. Reedijk J (1987) Comprehensive coordination chemistry, (Chapter 13.2), vol 2. Pergamon, Oxford
6. Wang SX, Yu SY, Luo QH (1994) Transition Met Chem 19:205–208
7. Horton DA, Bourne GT, Smythe ML (2003) Chem Rev 103: 893–931

8. Aminabhavi TM, Biradar NS, Patil SB, Hoffman DE (1986) Inorg Chim Acta 125:125–128
9. Cowan JA (1998) Chem Rev 98:1067–1088
10. Liu CL, Wang M, Zhang TL, Sun HZ (2004) Coord Chem Rev 248:147–168
11. Wu HL, Huang XC, Yuan JK, Kou F, Jia F, Liu B, Wang KT (2010) Eur J Med Chem 45:5324–5330
12. Wu HL, Li K, Sun T, Kou F, Jia F, Yuan JK, Liu B, Qi BL (2011) Transition Met Chem 36:21–28
13. Wu HL, Yun RR, Wang KT, Li K, Huang XC, Sun T (2010) Z Anorg Allg Chem 636:629–633
14. Wu HL, Huang XC, Yuan JK, Kou F, Chen GS, Jia BB, Yang Y, Lai YL (2010) Z Naturforsch B 65:1334–1340
15. Bukhari SB, Memon S, Mahroof-Tahir M, Bhanger MI (2009) Spectrochim Acta A Mol Biomol Spectrosc 71:1901–1906
16. Afanas'ev IB, Ostrakhovitch EA, Mikhal'lchi EV, Ibragimova GA, Korkina LG (2001) Biochem Pharma 61:677–684
17. Botelho FV, Alvarez-Leite JI, Lemos VS, Pimenta AMC, Calado HDR, Matencio T, Miranda CT, Pereira-Maia EC (2007) J Inorg Biochem 101:935–943
18. Wang Q, Yang ZY, Qi GF, Qin DD (2009) Eur J Med Chem 44:2425–2433
19. Satyanarayana S, Dabrowiak JC, Chaires JB (1993) Biochemistry 32:2573–2584
20. Reichmann MF, Rice SA, Thomas CA, Doty P (1954) J Am Chem Soc 76:3047–3053
21. Pyle AM, Rehmann JP, Meshoyrer R, Kumar CV, Turro NJ, Barton JK (1989) J Am Chem Soc 111:3051–3058
22. Wolf A, Shimer GH, Meehan T (1987) Biochemistry 26:6392–6396
23. Baguley BC, Bret ML (1984) Biochemistry 23:937–943
24. Lakowicz JR, Webber G (1973) Biochemistry 12:4161–4170
25. Tan CP, Liu J, Chen LM, Shi S, Ji LN (2008) J Inorg Biochem 102:1644–1653
26. Winterbourn CC (1981) Biochem J 198:125–131
27. Winterbourn CC (1979) Biochem J 182:625–628
28. Guo ZY, Xing RE, Liu S, Yu HH, Wang PB, Li CP, Li PC (2005) Bioorg Med Chem Lett 15:4600–4603
29. Takahashi K, Nishida Y, Kida S (1984) Polyhedron 3:113–116
30. Wu HL, Yun RR, Li K, Wang KT, Huang XC, Sun T (2009) Synth React Inorg Met Org Nano Met Chem 39:614–617
31. Bruker (2000) Smart saint and sadabs. Bruker Axs, Inc, Madison
32. Sheldrick GM (1996) SHELXTL. Siemens Analytical X-ray Instruments, Inc., Madison
33. Geary WJ (1971) Coord Chem Rev 7:81–122
34. Su CY, Kang BS, Du CX, Yang QC, Mak TC (2000) Inorg Chem 39:4843–4849
35. Lane TJ, Nakagawa I, Walter JL, Kandathil AJ (1962) Inorg Chem 1:267–276
36. Richard JS, Martin RB (1974) Chem Rev 74:471–517
37. Chec EK, Kubiak M, Glowiak T, Ziolkowski JJ (1998) Transition Met Chem 23:641–643
38. Fonseca T, Gigante B, Gilchrist TL (2001) Tetrahedron 57: 1793–1799
39. Wu HL, Wang KT, Yun RR, Huang XC (2009) Synth React Inorg Met Org Nano Met Chem 39:629–632
40. Su ZX, Wan YQ, Wu HL (2005) Synth React Inorg Met Org Nano Met Chem 35:553–558
41. Xiao LE, Zhang M, Sun WH (2010) Polyhedron 29:142–147
42. Kang D, Seo J, Lee SY, Lee JY (2007) Inorg Chem Comm 10:1425–1428
43. Yoshikawa N, Yamabe S, Kanehisa N, Kai Y, Takashima H, Tsukahara K (2007) Eur J Inorg Chem 13:1911–1919
44. Collin JP, Dixon IM, Sauvage JP, Williams JAG, Barigelletti F, Flamigni L (1999) J Am Chem Soc 121:5009–5016
45. Li H, Le XY, Pang DW, Deng H, Xu ZH, Lin ZH (2005) J Inorg Biochem 99:2240–2247
46. Vaidyanathan VG, Nair BU (2003) Eur J Inorg Chem 19:3633–3638
47. Vaidyanathan VG, Nair BU (2004) Eur J Inorg Chem 9: 1840–1846
48. Liu J, Zhang TX, Ji LN (2002) J Inorg Biochem 91:269–276
49. LePecq JB, Paoletti C (1967) J Mol Biol 27:87–106
50. Mahadevan S, Palaniandavar M (1998) Inorg Chem 37:693–700
51. Tossi AB, Kelly JM (1989) Photochem Photobiol 49:545–556
52. Satyanarayana S, Dabrowiak JC, Chaires JB (1992) Biochemistry 31:9319–9324
53. Li TR, Yang ZY, Wang BD, Qin DD (2008) Eur J Med Chem 43:1688–1695
54. Schepetkin I, Potapov A, Khlebnikov A, Korotkova E, Lukina A, Malovichko G, Kirpotina L, Quinn MT (2006) J Biol Inorg Chem 11:499–513
55. Patel MN, Gandhi DS, Parmar PA (2010) Inorg Chem Comm 13:618–621